

Preparation of Subradiant States using Local Qubit Control in Circuit QED

S. Filipp,^{1,*} A. F. van Loo,¹ M. Baur,¹ L. Steffen,¹ and A. Wallraff¹

¹*Department of Physics, ETH Zurich, CH-8093 Zurich, Switzerland*

Transitions between quantum states by photon absorption or emission are intimately related to symmetries of the system which lead to selection rules and the formation of dark states. In a circuit quantum electrodynamics setup, in which two resonant superconducting qubits are coupled through an on-chip cavity and driven via the common cavity field, one single-excitation state remains dark. Here, we demonstrate that this dark state can be excited using local phase control of individual qubit drives to change the symmetry of the driving field. We observe that the dark state decay via spontaneous emission into the cavity is suppressed, a characteristic signature of subradiance. This local control technique could be used to prepare and study highly correlated quantum states of cavity-coupled qubits.

PACS numbers: 42.50.Ct, 03.67.Lx, 42.50.Pq, 85.35.Gv

Symmetry properties of a quantum system interacting with a radiation field provide information about possible transitions within the system. Symmetry operations such as translation, rotation or reflection which leave the system invariant, lead to selection rules in molecular and solid-state systems [1]. For an ensemble of identical atoms, the symmetry under permutation of particles allows only for transitions between symmetric collective states [2, 3]. Such highly-entangled Dicke-states, like the single-excitation W-state, have attracted a lot of attention in the field of quantum information processing with trapped ions [4], optical photons [5] or superconducting qubits [6] due to their robustness under decoherence [7] and particle loss [8, 9]. Moreover, collective states have been used for quantum information storage in atomic memories [10]. The particular symmetry of Dicke states affects also their decay. Spontaneous emission can be enhanced for superradiant states [2, 3], or inhibited, if the symmetry of the state does not allow for the emission of a photon. This effect is known as subradiance and is closely related to the concept of decoherence-free subspaces, regions in Hilbert space which are not affected by decoherence and therefore appealing for quantum information processing [11]. Though theoretically well studied [12, 13], subradiant states are difficult to realize and experimental evidence of subradiance is rare [14, 15].

Here we present a method to prepare two qubits in antisymmetric Dicke states and demonstrate their subradiance in circuit quantum electrodynamics (QED) [16, 17]. In this architecture, superconducting artificial atoms are coupled to a common field mode of a planar microwave cavity. Strong resonant coupling of individual qubits [18–20] and qubit-ensembles [21] to single microwave photons has been achieved. Moreover, cavity-mediated interactions between distant qubits [22–24] form the basis for on-chip quantum information processing [25, 26] using entangled states of currently up to three qubits [27]. In many experiments, the qubits are detuned from the cavity resonance. In this dispersive regime, the cavity can be used for the preparation and read-out of entangled

states [28, 29], and cavity induced radiative decay of the qubits due to the Purcell effect [30] is reduced. This enhanced spontaneous emission can be modified by the qubit-cavity detuning [31] and is the dominant relaxation mechanism close to resonance. We have observed subradiance by preparing an antisymmetric two-qubit state in this regime using local phase control to change the symmetry of the driving field [Fig. 1(a)].

We consider two qubits resonant with each other but not with the cavity, modeled by a generalized Tavis-Cummings Hamiltonian [32],

$$H_{\text{TC}}/\hbar = \omega_r a^\dagger a + \omega_q J_z + g(aJ_+ + a^\dagger J_-). \quad (1)$$

where the dominant cavity mode is at frequency ω_r and the qubits are at frequency ω_q . The operators $J_\pm \equiv 1/2 \sum_i^N \sigma_\pm^{(i)}$ and $J_\pm \equiv \sum_i^N \sigma_\pm^{(i)}$ are collective spin operators [3] with $\sigma_\pm^{(i)} \equiv (\sigma_x^{(i)} \pm i\sigma_y^{(i)})/2$ and Pauli operators $\sigma_{x,y,z}^{(i)}$ for the individual qubits ($i = 1, 2$). $a^{(\dagger)}$ is the annihilation (creation) operator of the field interacting with the qubits with equal coupling strength g . For the single-excitation manifold the eigenstates of H_{TC} are

$$\begin{aligned} |\psi_a\rangle &= |0; \psi_-\rangle, \\ |\psi_r\rangle &= \cos \theta_m |1; gg\rangle + \sin \theta_m |0; \psi_+\rangle, \\ |\psi_s\rangle &= \sin \theta_m |1; gg\rangle - \cos \theta_m |0; \psi_+\rangle, \end{aligned} \quad (2)$$

where the mixing angle θ_m is given by $\cos 2\theta_m = -\Delta/\sqrt{4(\sqrt{2}g)^2 + \Delta^2}$. $|n;\rangle$ is a state with n photons in the resonator, and $|\psi_\pm\rangle = (|ge\rangle \pm |eg\rangle)/\sqrt{2}$ are the symmetric and antisymmetric Bell-states. The qubit-resonator detuning $\Delta \equiv \omega_q - \omega_r$ is chosen negative. The antisymmetric state $|\psi_a\rangle$ – comprising the antisymmetric qubit state $|\psi_-\rangle$ – does not couple to the cavity field. Only the symmetric qubit state $|\psi_+\rangle$ mixes with the field to form hybridized matter-field states $|\psi_r\rangle$ and $|\psi_s\rangle$ [Fig. 1(b)] with enhanced collective coupling strength $\sqrt{N}g$ for $N = 2$ [21]. Generally, for an N -qubit ensemble there are always two hybridized bright states and $N - 1$

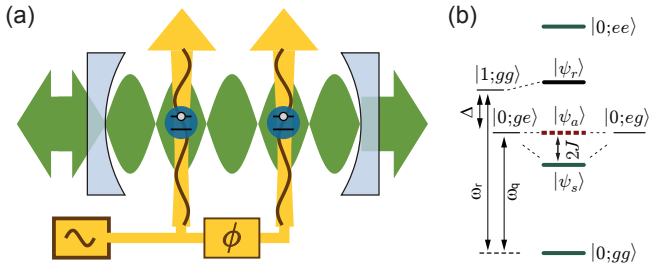


FIG. 1: (a) Schematic drawing of a cavity QED setup with individual phase control of the driving field for each (artificial) atom. (b) Energy level diagram of the two-qubit system coupled dispersively to a common cavity field. Symmetric states are indicated by thick solid (green) lines and the antisymmetric state is identified by the thick dashed (red) line.

uncoupled, dark states. Only qubit states which reflect the symmetry of the cavity mode (i. e. belong to compatible irreducible representations of the permutation group [12]) couple to the single-photon field. In our case, the coupling to the first harmonic cavity mode has the same sign for both qubits ($g^{(1)} \approx g^{(2)}$) [24]. Therefore, the symmetric qubit state $|\psi_s\rangle$, which is invariant under permutation of the qubits, couples to the field.

For our experiments, two superconducting transmon qubits [33] have been integrated into a coplanar niobium resonator on a sapphire substrate [Fig. 2(a,b)]. The qubits have similar Josephson energies $E_J/h \approx 37.6$ GHz, charging energies $E_C/h \approx 285$ MHz and coupling strengths $g/2\pi \approx 116$ MHz to the first harmonic mode of the microwave transmission line resonator. The resonator frequency is $\omega_r/2\pi = 6.937$ GHz and its decay rate is $\kappa/2\pi = 3.01$ MHz. In the dispersive regime where $\theta_m \approx \pi$, the photonic contribution $|1;gg\rangle$ to the symmetric state $|\psi_s\rangle$ is small (of order $\sqrt{2}g/\Delta$) and the state has pre-dominantly qubit character. It is however, shifted in energy by $2J \equiv 2g^2/\Delta$ corresponding to the dispersive J -coupling discussed in Refs. [22, 24] [Fig. 1(b)]. The antisymmetric wave-function $|\psi_a\rangle$ has no photonic component and thus experiences no Lamb-shift of its energy. In this description the qubit-qubit coupling J can be understood as the collective Lamb-shift $(\sqrt{2}g)^2/\Delta = 2J$ of the symmetric state $|\psi_s\rangle$.

The symmetry of these states is also reflected in selection rules for electric dipole transitions. In fact, for a drive applied directly to the cavity only, transitions from the ground to the symmetric bright state $|\psi_s\rangle$ are allowed, while transitions to the antisymmetric dark state $|\psi_a\rangle$ are forbidden [24]. Again, this is due to identical microwave fields at the qubit positions for a drive close to the first harmonic cavity mode, which conserves the symmetry under permutation of qubits. Then only transitions within the class of symmetric states [Fig. 1(b); solid green lines] are allowed [12]. This constraint can be overcome by addressing the qubits individually via capac-

itively coupled charge lines [28] and tuning the relative phase ϕ of the microwave drive at the qubit positions. When choosing a relative phase of $\phi = \pi$, the opposite sign of the local fields results in allowed transitions to the antisymmetric state [42].

In the rotating frame, the drive acting on the individual qubits with frequency ω_d and coupling ϵ is

$$H_d = \hbar\epsilon \left(\sigma_+^{(1)} + \xi e^{i\phi} \sigma_+^{(2)} \right) + h.c., \quad (3)$$

where ξ is the amplitude imbalance at the individual qubits. Starting in the ground state, the drive H_d can induce transitions to the state $|\psi\rangle$, if the matrix element $\Omega(\psi) \equiv |\langle 0;gg|H_d|\psi\rangle|/\hbar$ is non-zero. $\Omega(\psi_{\text{dark}}) = 0$, therefore, defines the dark state for given drive imbalance ξ and relative phase ϕ . In the dispersive regime, the matrix element for the symmetric and antisymmetric state is

$$\Omega(\psi_{s/a}) = \epsilon \sqrt{(1 + \xi^2 \pm 2\xi \cos \phi)/2}. \quad (4)$$

For equal drive amplitudes ($\xi = 1$) and zero relative phase ($\phi = 0$), which corresponds to a drive applied to the cavity in the vicinity of the first harmonic mode, $\Omega(\psi_a)$ vanishes and the antisymmetric state $|\psi_a\rangle$ remains dark [24]. For $\phi = \pi$ and $\xi = 1$ however, $\Omega(\psi_a)$ is maximal, while the transition rate $\Omega(\psi_s)$ to the symmetric state vanishes. The transition can thus be enabled, or disabled, by adjusting the relative phase appropriately.

We have spectroscopically measured the transition amplitude as a function of relative phase ϕ in the vicinity of the bare qubit frequency $\omega_q/2\pi = 6.647$ GHz. To control ϕ , the local microwave fields are generated by a single microwave source operating at the carrier frequency $\omega_{\text{LO}} = \omega_d + \omega_{\text{IF}}$. We use two in-phase/quadrature (IQ) mixers to generate sidebands of the carrier signal at the frequency ω_d . The signal (IF) at the intermediate frequency $\omega_{\text{IF}} = 150$ MHz is synthesized with an arbitrary waveform generator and applied to each mixer with relative phase ϕ [Fig. 2(a)]. The phase ϕ of the local qubit drive fields can then be controlled with high

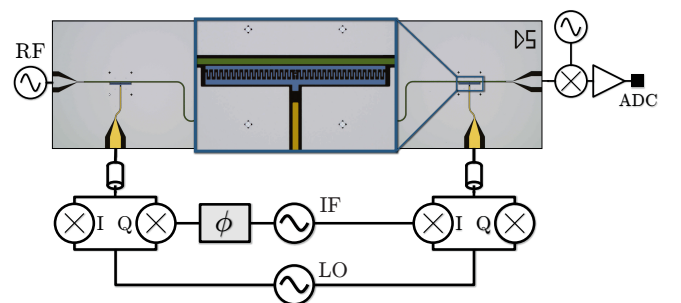


FIG. 2: Setup and micrograph of the sample with a transmission line resonator (green) and two transmon qubits (blue) addressable via local charge lines (yellow).

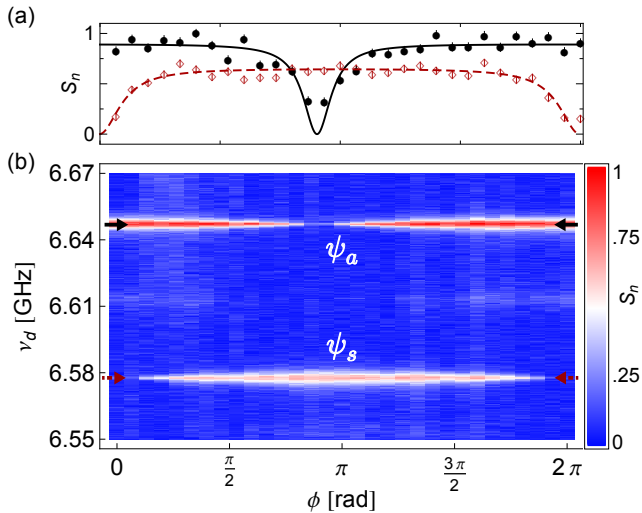


FIG. 3: Spectroscopy of dark and bright state as a function of the relative phase ϕ between drives. (a) Normalized integrated transmission amplitudes $S_n = S/S_{\max}$ of the antisymmetric state ψ_a (black solid dots) and the symmetric state ψ_s (red open diamonds) at the frequencies $\omega_a/2\pi = 6.647$ GHz and $\omega_s/2\pi = 6.578$ GHz, respectively, as indicated by the arrows in (b). S_n is normalized to unity at the maximum value of both curves S_{\max} . The lines indicate fits to the expected steady-state populations. (b) Transmission amplitude as a function of frequency ν_d and relative phase ϕ .

precision by the phase of the IF-signals. Pulsed spectroscopy is used [34, 35], where the measurement tone is switched on after a 500 ns saturation pulse [Fig. 3(a)]. The difference between the transmitted signal $s(t)$ and the signal with both qubits in their ground state $s_{gg}(t)$ integrated over $t_m = 520$ ns yields the transmission amplitude $S = \int_0^{t_m} \{s(t) - s_{gg}(t)\} dt$. S corresponds to a measurement of the steady-state population of the single-excited qubit states when appropriately normalized [29].

Two spectroscopic lines, varying in amplitude as a function of relative phase ϕ , are observed at $\omega_a/2\pi = 6.647$ GHz and $\omega_s/2\pi = 6.578$ GHz. These correspond to the states $|\psi_a\rangle$ and $|\psi_s\rangle$, respectively. As expected, the zeros of the populations of the symmetric and the antisymmetric state are 180° out-of-phase [Fig. 3]. The measured transmission amplitudes are in good agreement with the steady-state population of the excited states calculated using the dissipative Bloch equations for a two-level system driven at zero detuning [36], $S = S_0 \{1 - 1/(1 + T_1 T_2 \Omega(\psi)^2)\} / 2$. The scaling factor S_0 takes account of the integrated voltage at the analog-digital converter. The dephasing times $T_{2,s} = 322 \pm 26$ ns and $T_{2,a} = 526 \pm 36$ ns of $|\psi_s\rangle$ and $|\psi_a\rangle$ are determined in independent Ramsey-fringe experiments. The energy relaxation times $T_{1,s}$ and $T_{1,a}$ are measured in separate time-delay experiments and are discussed below. From independent fits of S to both curves we obtain the relative phase difference between the zeros of the popu-

lations of the symmetric and the antisymmetric state $\phi_s - \phi_a = \pi - 0.3 \pm 0.03$ rad using $\Omega(\psi_{s/a})$ from Eq. (4). The deviation of the measured phase difference from π is simply caused by the difference in cable lengths of the two qubit drive lines.

Using this method, it is possible to verify the subradiant character of the antisymmetric state by testing its resilience to cavity-induced Purcell decay [30], which is caused by the indirect coupling of the qubits to the environment via the cavity. According to Fermi's golden rule, the induced voltage fluctuations $\propto (a^\dagger + a)$ of the cavity field lead to a decay rate $\gamma_\kappa = \kappa |\langle 0; gg|a|\psi \rangle|^2$ to the ground state [18, 33]. The total decay rate is then given by $\gamma = \gamma_i + \gamma_\kappa$ with the intrinsic, non-radiative decay rate γ_i . Although the Purcell decay can be made small by operating the qubits in the dispersive regime, where $\gamma_\kappa \approx (g/\Delta)^2 \kappa$, or by using advanced circuit designs [37], it cannot be fully avoided for single transmon qubits. For the dark state however, the matrix element $|\langle 0; gg|a|\psi_a \rangle|$ vanishes completely, since by symmetry $|\psi_a\rangle$ has no photon admixture. In other words, destructive interference of the photons emitted from either qubit leads to a suppression of the spontaneous emission process and the dark state is protected against Purcell decay. Note that a two-island transmon design, in essence the integrated version of the two-qubit/cavity circuit used in the experiments discussed here, also provides Purcell-protection based on the formation of an intrinsic dark state [38, 39].

In order to observe subradiant Purcell-protection in a regime where radiative losses dominate over intrinsic qubit losses ($\gamma_\kappa > \gamma_i$), we have detuned the qubits from the first harmonic mode by $\Delta/2\pi = 290$ MHz $\sim 2.5g$. At this frequency, the lifetime of the symmetric and antisymmetric state, as well as the decay rates of the individual qubits have been measured. A delayed measurement pulse technique has been employed, where we apply a π pulse resonant with the respective transition frequency and delay the time Δt before applying the read-out pulse. The lifetimes of single qubit excitations $T_{1,ge} = 401 \pm 16$ ns and $T_{1,eg} = 364 \pm 16$ ns at this frequency are comparable to the bright state lifetime of $T_{1,s} = 368 \pm 30$ ns. In our measurements, the effect of superradiant decay is masked by the intrinsic decay rate and by dephasing acting locally on individual qubits. In contrast, the measured dark state lifetime $T_{1,a} = 751 \pm 13$ ns exceeds these values by a factor of two – a clear signature of subradiance that demonstrates the decoupling of the antisymmetric state from the cavity environment and, as a consequence, its enhanced stability. The population decay versus time of both the bright and the dark state is plotted in Fig. 4(a).

The lifetime of the dark state is shown at different detunings, along with the lifetimes of the bright state and the uncoupled single qubit states in Fig. 4(b). It is verified in numerical master equation simulations of the dissipative dynamics for ψ_a [Fig. 4(b); solid black line] and

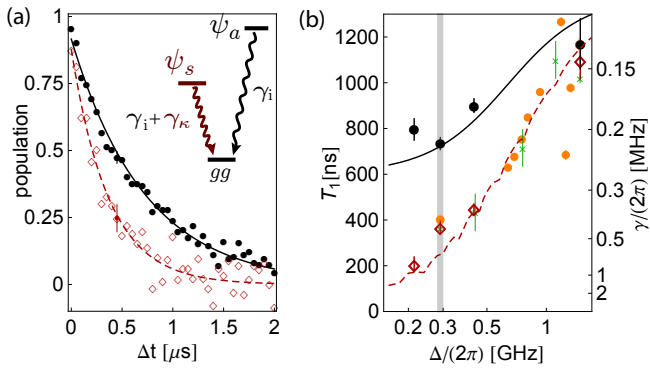


FIG. 4: (a) Population of the antisymmetric dark (ψ_a , black dots) and the symmetric bright (ψ_s , red diamonds) state versus time at $\Delta/2\pi = 290$ MHz (gray line in (b)) with exponential fits to the data. The inset shows the energy relaxation from ψ_a and ψ_s to the ground state, where only the symmetric state ψ_s is affected by the Purcell decay γ_κ . (b) Measured decay times of ψ_s (red diamonds), ψ_a (black dots) and the uncoupled qubit states eg (orange points) and ge (green crosses) as a function of detuning Δ . Exponential fits to numerically simulated populations are shown for ψ_s (dashed line) and ψ_a (solid line).

ψ_s [Fig. 4(b); dashed red line] that the decreasing lifetime of the dark state at small detunings is caused by local dephasing. For these simulation, a pure dephasing time of $T_{2,\phi} = 880$ ns has been determined in Ramsey-fringe experiments of the uncoupled qubits with an intrinsic decay time of $1.37 \mu\text{s}$ obtained from a fit to $T_{1,eg}(\Delta)$.

The enhanced dark-state lifetime can be used for quantum computation. In fact, the logical qubit formed by the ground and the dark state realizes a decoherence-free subspace, which is insensitive to cavity dissipation as well as to global dephasing acting simultaneously on both qubits. Note however, that the subspace spanned by $|0; gg\rangle$, $|\psi_a\rangle$ and the doubly excited state $|0; ee\rangle$ forms a weakly nonlinear qubit with anharmonicity $2J$, which limits the shortest preparation time without pulse optimization [40] to $\sim 1/(2J)$.

More generally, this local control technique may allow us to excite highly entangled Dicke states belonging to different symmetry classes with a single microwave pulse conditioned on the choice of phases between individual drives. Moreover, the possibility to address states of different symmetry classes of multi-qubit systems can be used to encode information in collective qubit states. For readout, they can be transformed into entangled states in the computational basis by rapidly detuning the qubit transition frequencies.

In conclusion, we have demonstrated a method to populate dark states of a two-qubit system in a circuit QED setup. The transitions to either dark or bright two-qubit states can be selected by adjusting the relative phase between individual qubit drives, thus changing the symmetry of the field and enforcing a symmetry-induced se-

lection rule. We apply this technique to demonstrate Purcell-protection of the subradiant dark state against spontaneous emission. An extension to more qubits could provide further insight into the unitary and dissipative dynamics of multi-particle quantum states that can be directly prepared in the coupled qubit basis. Controlling the symmetry of the radiation field is, therefore, a viable method for preparation of states that are otherwise difficult to realize.

This work was supported by the Swiss National Science Foundation (SNF). S.F. acknowledges support by the Austrian Science Foundation (FWF). The authors thank A. Blais and J. Gambetta for valuable discussions.

* Electronic address: filipp@phys.ethz.ch

- [1] W. Ludwig and F. C., *Symmetries in Physics: Group Theory Applied to Physical Problems* (Springer, 1988).
- [2] R. H. Dicke, *Phys. Rev.*, **93**, 99 (1954).
- [3] M. Gross and S. Haroche, *Phys. Rep.*, **93**, 301 (1982).
- [4] H. Häffner, et al., *Nature*, **438**, 643 (2005).
- [5] M. Eibl, et al., *Phys. Rev. Lett.*, **92**, 077901 (2004).
- [6] M. Neeley, et al., *Nature*, **467**, 570 (2010).
- [7] O. Gühne, F. Bodoky, and M. Blaubaer, *Phys. Rev. A*, **78**, 060301 (2008).
- [8] W. Dür, G. Vidal, and J. I. Cirac, *Phys. Rev. A*, **62**, 062314 (2000).
- [9] H. J. Briegel and R. Raussendorf, *Phys. Rev. Lett.*, **86**, 910 (2001).
- [10] N. Sangouard, C. Simon, H. de Riedmatten, and N. Gisin, *Rev. Mod. Phys.*, **83**, 33 (2011).
- [11] D. A. Lidar and K. B. Whaley, in *Irreversible Quantum Dynamics*, edited by F. Benatti and R. Floreanini (Springer, 2003), *Lecture Notes in Physics 622*, 83–120.
- [12] A. Crubellier, S. Liberman, D. Pavolini, and P. Pillet, *J. Phys. B*, **18**, 3811 (1985).
- [13] A. Crubellier and D. Pavolini, *J. Phys. B*, **19**, 2109 (1986); A. Crubellier, *J. Phys. B*, **20**, 971 (1987); A. Crubellier and D. Pavolini, *J. Phys. B*, **20**, 1451 (1987).
- [14] D. Pavolini, et al., *Phys. Rev. Lett.*, **54**, 1917 (1985).
- [15] R. G. DeVoe and R. G. Brewer, *Phys. Rev. Lett.*, **76**, 2049 (1996).
- [16] A. Wallraff, et al., *Nature*, **431**, 162 (2004).
- [17] A. Blais, et al., *Phys. Rev. A*, **69**, 062320 (2004).
- [18] A. Houck, et al., *Nature*, **449**, 328 (2007).
- [19] J. M. Fink, et al., *Nature*, **454**, 315 (2008).
- [20] D. Bozyigit, et al., *Nat. Phys.*, **7**, 154 (2011).
- [21] J. M. Fink, et al., *Phys. Rev. Lett.*, **103**, 083601 (2009).
- [22] J. Majer, et al., *Nature*, **449**, 443 (2007).
- [23] F. Altomare, et al., *Phys. Rev. B*, **82**, 094510 (2010).
- [24] S. Filipp, et al., *Phys. Rev. A*, **83**, 063827 (2011).
- [25] L. DiCarlo, et al., *Nature*, **460**, 240 (2009).
- [26] H. Wang, et al., arXiv:1011.2862 (2010).
- [27] L. DiCarlo, et al., *Nature*, **467**, 574 (2010).
- [28] P. J. Leek, et al., *Phys. Rev. B*, **79**, 180511 (2009).
- [29] S. Filipp, et al., *Phys. Rev. Lett.*, **102**, 200402 (2009).
- [30] E. M. Purcell, *Phys. Rev.*, **69**, 681 (1946).
- [31] A. A. Houck, et al., *Phys. Rev. Lett.*, **101**, 080502 (2008).
- [32] M. Tavis and F. W. Cummings, *Phys. Rev.*, **170**, 379

- (1968).
- [33] J. Koch, et al., Phys. Rev. A, **76**, 042319 (2007).
 - [34] A. Wallraff, et al., Phys. Rev. Lett., **95**, 060501 (2005).
 - [35] R. Bianchetti, et al., Phys. Rev. A, **80**, 043840 (2009).
 - [36] A. Abragam, *Principles of Nuclear Magnetism* (Oxford University Press, 1961).
 - [37] M. D. Reed, et al., Appl. Phys. Lett., **96**, 203110 (2010).
 - [38] J. M. Gambetta, A. A. Houck, and A. Blais, Phys. Rev. Lett., **106**, 030502 (2011).
 - [39] S. J. Srinivasan, A. J. Hoffman, J. M. Gambetta, and A. A. Houck, Phys. Rev. Lett., **106**, 083601 (2011).
 - [40] F. Motzoi, J. M. Gambetta, P. Rebentrost, and F. K. Wilhelm, Phys. Rev. Lett., **103**, 110501 (2009).
 - [41] P. C. de Groot, et al., Nat. Phys., **6**, 763 (2010).
 - [42] Recently, amplitude and phase control has also been used to suppress transitions in a two flux qubit system [41].